Chapter 4

Hydrogenation cleans up airborne contamination from graphene

Graphene as a two-dimensional surface is prone to airborne contaminations, which can significantly impact surface-related properties including electrochemistry and wettability. Here, by combining multiscale characterization techniques, hydrogenation treatment as a non-invasive strategy is demonstrated to remove the hydrocarbon contamination from the graphene surface while preserving graphene crystallinity. The hydrogenated graphene manifests enhanced water adsorption as compared to its pristine state, resulting in a protective layer against the redeposition of hydrocarbon molecules. Our findings provide a new strategy for graphene to maintain its surface cleanliness, inherently improving performance in biosensing and interfacing applications.

This chapter was prepared as an article: Lin Jiang, Pauline M.G. van Deursen, Hadi Arjmandi-Tash, Liubov A. Belyaeva, Haoyuan Qi, Jiao He, Vincent Kofman, Longfei Wu, Valerii Muravev, Ute Kaiser, Harold Linnartz, Emiel J.M. Hensen, Jan P. Hofmann, Grégory F. Schneider, submitted.

4.1 Introduction

Cutting-edge applications involving a graphene surface require a clean surface and a precise knowledge of the chemical structure of the basal plane. However, surface contaminations introduced during device fabrication processes can have a significant and unpredictable impact on the electrical and electrochemical properties of graphene. For chemical vapor deposition (CVD) graphene, the majority of the accumulated contaminations originate from the transfer-assisting polymer (typically poly(methyl methacrylate), PMMA). To date, many efforts have been devoted to removing PMMA residues, i.e. with the use of annealing in vacuum or specific atmospheres (air or H_2/Ar mixture)[1], mechanical removal of contaminants by AFM scanning[2], current cleaning[3], electrostatic force cleaning[4] or plasma dry-cleaning[5]. In particular, hydrogen plasma has been intensively studied for patterning and etching graphite surfaces.[6] By tuning the energy of the involved hydrogen species impinging on the surfaces one can control and customize, in principle, the morphology and functionalization of graphene.[7]

In previous work, we showed that the electrochemical activity of graphene can be enhanced by just one second of hydrogen plasma treatment, but decreases with prolonged hydrogenation.[8] The decrease of electrochemical activity can attributed to changes in the electronic structure of the graphene layer. According to non-adiabatic theory for electron transfer, decreasing electrochemical activity is due to the reduction of the density of states (DOS) in graphene. On the other hand, the electrochemical activity improvement – by up to 12-fold after one second of hydrogenation – is expected to be related to the removal of airborne hydrocarbons at the graphene surface. Airborne contaminations mainly composed of various hydrocarbons, are pervasive in the ambient conditions, and can adsorb onto graphene via hydrophobic interactions to form an amorphous coating.[9] However, few efforts have been devoted to removing airborne hydrocarbons,[9] despite the influence of those hydrocarbons on the wettability and even the electrochemical kinetics of the surface of graphene or graphite.[10] Such uncontrolled surface chemistry and substantial variation in electrical performances of graphene pose significant challenges which remain to be solved.

Here, the cleaning effect upon hydrogenation is demonstrated to result in graphene with well-maintained lattice integrity and crystallinity, as confirmed using aberration-corrected high-resolution transmission electron microscopy (AC-HRTEM). Further statistical analysis of the TEM images quantitatively evaluates the cleanliness of graphene surfaces, defined as the proportion of the area on the crystalline lattice without amorphous coverage in TEM images. Specifically the focus

is on water adsorption, which has been reported to act in concert with hydrogenation and effectively impacts the doping behavior in graphene.[11] Furthermore, chemical water adsorption was confirmed to potentially minimize hydrocarbon contaminations at graphitic surfaces.[12] As a result, it is hypothesized that in addition to chemically modifying the basal plane from sp^2 to sp^3, hydrogenation also cleans graphene by removing surface adsorbed hydrocarbons, and preserves the cleanliness through the adsorption of a water protecting layer. Thus, hydrogenation can effectively improve the anti-fouling capability of the graphene basal plane towards airborne contaminations. This process is further studied using temperature programmed desorption-infrared spectroscopy (TPD-IR) and near-ambient pressure X-ray photoelectron spectroscopy (NAP-XPS) confirming the preferred adsorption of water at the hydrogenated graphene surface.

4.2 Results

4.2.1 High resolution transmission electron microscopy (HRTEM)

The surface morphology of graphene films grown by CVD method[13] was studied by AC-HRTEM, to compare the effects of hydrogen and argon plasma on surface cleanliness. A capacitively coupled plasma system (Diener electronic, Femto) was used to form mild plasma via tuning the power and gas pressures. Three types of graphene treatments are investigated: 1) hydrogen-treated graphene (H-graphene), 2) argon treated graphene (Ar-graphene), 3) as-synthesized graphene without plasma exposure ("pristine" graphene). For a fair and reliable comparison, both the H- and Ar-graphene contain similar amounts of corresponding H or vacancy defects[8], confirmed by Raman spectroscopy (Figure AIII. 1). Figure 4.1a shows the HRTEM image of H-graphene exposed to hydrogen plasma for 60 seconds, in which the first-order reflections of graphene are clearly visible in the fast Fourier transform (FFT) pattern. The amorphous residuals are surface contaminations, originating from the preparation procedures (unavoidable solvents or aqueous solutions) and airborne hydrocarbons.[9] By introducing the same amount of defect density, argon plasma was tested as a control to further confirm the cleaning effect. In contrast to the HRTEM image of pristine graphene in Figure AIII. 2, both H-graphene and Ar-graphene graphene show improved cleanliness. Compared to the one treated with argon plasma (Ar-graphene) (Figure 4.1b), a cleaner graphene lattice with less coverage of amorphous carbon has been found in hydrogenated graphene (H-graphene) (Figure 4.1a). Particularly, a close-up of Figure 4.1a-b presented in Figure 4.1c-f clearly shows the atomically resolved graphene lattice, confirming the relatively larger area of clean and preserved surface crystallinity in H-graphene. Different from the visible hole/vacancy[14] formed in Ar-graphene (Figure 4.1f), a point defect in H-graphene is suspected to be related to the hydrogenation or the damage by the electron beam during imaging (Figure 4.1e). As

a result, the hypothesis is that, without sacrificing the integrity and crystallinity, hydrogenation cleans off the amorphous contaminants on the graphene surface while uniformly hybridizing graphene lattice from sp^2 to sp^3.

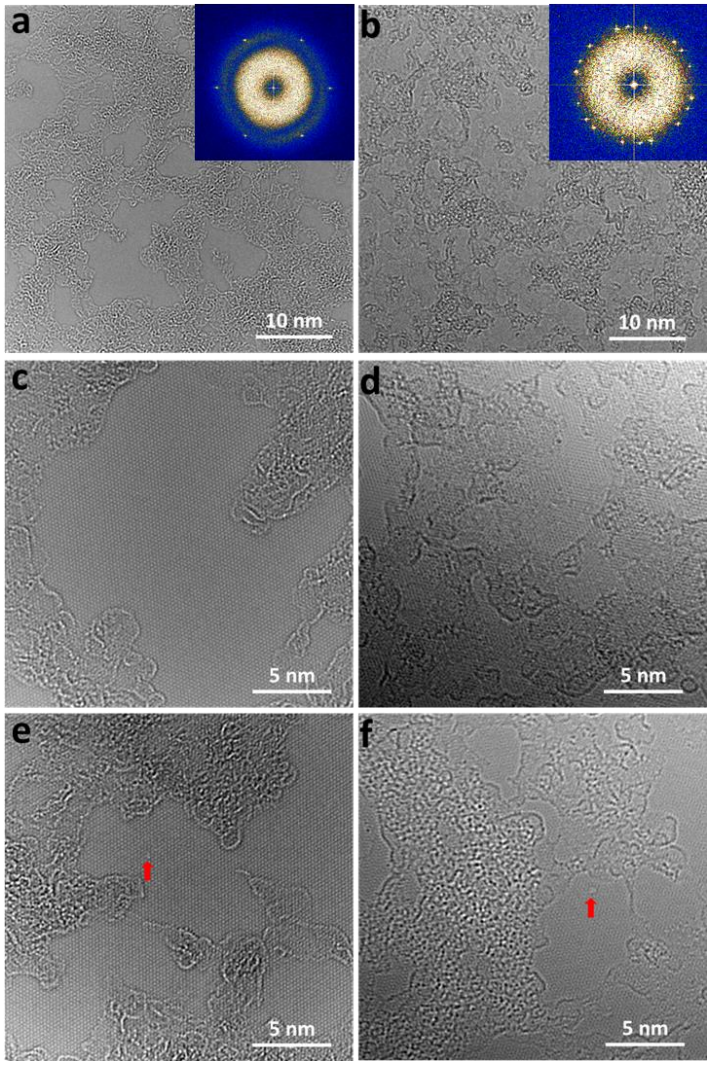

Figure 4.1 Comparison of graphene surfaces upon hydrogen vs argon plasma treatments by high resolution transmission electron microscopy (HRTEM). a) HRTEM image of graphene after 60 s of hydrogenation (H-graphene). The inset FFT pattern shows six reflections 4.7 nm^{-1}, demonstrating the preservation of graphene crystallinity. b) HRTEM image of graphene bombarded for 13 s of argon plasma (Ar-graphene). The FFT with 18 reflections suggests a trilayer-like graphene stack with 3 orientations. c) A zoomed-in HRTEM image of the H-graphene. d) A zoomed-in HRTEM image of the Ar-graphene. e) HRTEM image of H-graphene with visible lattice defect indicated by the red arrow. f) HRTEM image of Ar-graphene with a void indicated by the red arrow.

4.2.2 Quantitative analysis of the cleanliness of hydrogenated graphene

To gain quantitative insights into the cleaning effect upon hydrogenation, a statistical analysis of the TEM images of graphene acquired with a larger field-of-view was performed. For H-graphene (Figure 4.2a, 60 s of hydrogenation), contaminations appear in patterns with more rough sites while clean lattice being more smooth. By converting the TEM image into a black-white binary image, the cleanliness within the field-of-view can be quantitatively evaluated. A MATLAB script (see Appendix III. 2) was developed to process TEM micrographs and to identify the surface contaminations automatically. Table AIII. 1 details the process within the script. Figure 4.2a illustrates a selected region in the TEM image of H-graphene before (left) and after (right) image processing. The black pixels in the right panel correspond to the identified contaminations in graphene. Using the processed images, the graphene "cleanliness" is defined as the ratio of clean area in the image. Specifically, the cleanliness of the image is calculated as the sum of the number of white pixels (clean graphene area) normalized by the total number of pixels.

Figure 4.2b shows the contrast of the general cleanliness between the surfaces of pristine and H-graphene. Based on a statistical analysis of 15 images for the two types of surfaces, the quantitative evaluation of the cleanliness is summarized in Figure 4.2c. Both the narrower distribution around the average and clearly higher values of cleanliness indicate that contaminations on the surface of H-graphene are considerably less. Moreover, the amorphous contaminations exhibit a more homogeneous morphology after hydrogenation.

Hydrogen plasma has been found previously to be able to remove polymer (i.e. poly-methyl-methacrylate) that is prone to leave residues on graphene.[5a, 5c] Here for the first time the cleaning effect of hydrogenation is demonstrated towards hydrocarbon contaminations adsorbed on graphene surfaces. In our previous study on H-graphene[8], an hydrogenation-induced p-doping effect was reported, which can be ascribed to surface adsorbed water. In addition, H-graphene was reported to show n-doping behavior after heating the sample in vacuum.[11] More unambiguous proof of the presence of adsorbed water on graphene surfaces and its cleaning effect towards the ubiquitous airborne contaminations is still lacking.

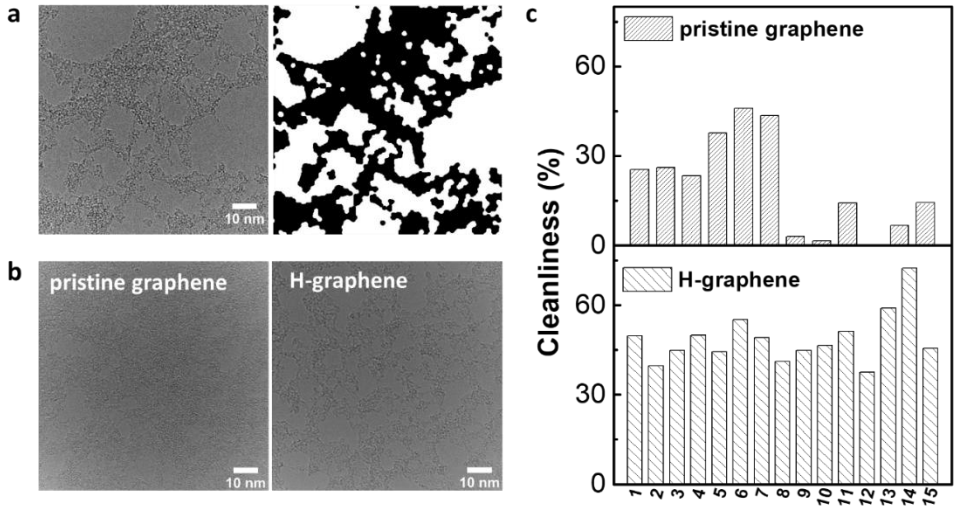

Figure 4.2 Quantitative analysis of graphene cleanliness in TEM images. a) TEM image of H-graphene (60 s) and its corresponding binary image distinguishing the clean and contaminated areas with white and black colors. The cleanliness (~52%) can be estimated based on the white pixels divided by the overall pixels. b) TEM image of pristine graphene and H-graphene upon 60 s of hydrogenation. c) Quantitative statistics of the cleanliness of graphene and hydrogenated graphene for 15 separate measurements.

4.2.3 Temperature programmed desorption-Infrared spectroscopy (TPD-IR)

To further understand the cleaning effect of hydrogenation and water adsorption on graphene, temperature-programmed desorption-infrared spectroscopy (TPD-IR) was performed. For this, a graphene sample was transferred via a biphasic polymer–free transfer method[15] on one side of an IR-transparent BaF_2 window that is mounted on the tip of a 15 K cryostat, positioned in the center of a high vacuum (HV) chamber in which the measurements were performed.[16] The HV chamber has a base pressure of 5×10^{-9} mbar when the cryostat is on, and residual gas in the chamber is dominated by H_2O and H_2. Sample temperatures are set with ~2 K precision using thermocouples and a temperature controller. It should be noted that the temperature during water deposition is intentionally set to be higher than the typical thermal desorption temperature of water ice (~160 K), ensuring that water ice does not build up on the sample. The monolayer quality and lattice integrity of the transferred pristine and H-graphene are confirmed by the sharp and single-Lorentz fitted 2D peak (~2670 cm^{-1}) of the Raman spectra in the inset of Figure 4.3a-b. Specifically, the peak at 1350 cm^{-1}, an indicator of the presence and density of defects in graphene lattice, is confirmed to be more intensive for H-graphene.

After the cryostat cooled down, the sample was heated to 324 K (highest accessible temperature) to degas any water potentially adsorbed to the sample during transfer through the atmosphere. Next the sample was cooled down to 180 K; at this stage any water adsorption is expected to happen through accretion from the background gas. During water deposition, almost no change was observed in the IR spectra, indicating that during cooling from 324 K to 180 K, the graphene surface was already water saturated. Further exposure to water did not lead to a further increase of H_2O related bands in the IR spectra. After water deposition, the sample was heated up with a linear ramp rate of 3 K per minute to 324 K to desorb the water from graphene. IR spectra were collected during the heating process.

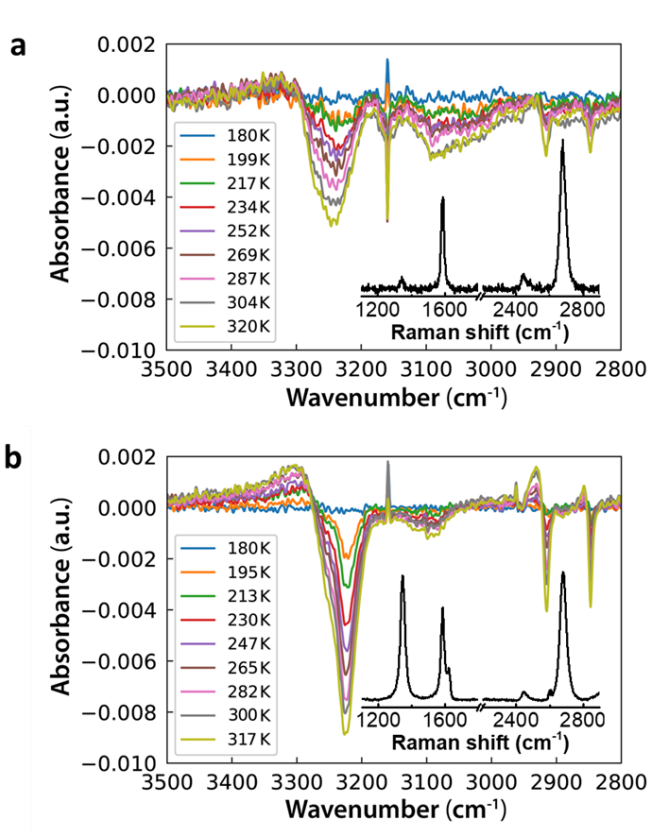

Figure 4.3 Water adsorption tests on graphene surfaces characterized by temperature-programmed desorption-infrared spectroscopy (TPD-IR). a) IR spectrum of pristine graphene for temperatures increasing from 180 to 320 K with increments of 15 to 20 K. b) IR spectrum of H-graphene (60 s) during a ramp-up in temperature from 180 to 317 K. All graphene samples are deposited on a BaF_2 window via a polymer-free transfer method. The inset corresponds to Raman spectrum of pristine and H-graphene on a barium fluoride substrate, respectively.

Figure 4.3 shows the IR absorption spectra of the pristine and H-graphene during heating up from 180 K to 324 K. Each spectrum was calculated with respect to the background scan performed at 180 K to obtain the desorption signals (see background spectrum in Figure AIII. 3a-b). Two peaks appear at ~2924 and ~2852 cm^{-1}, corresponding to the stretching mode of the C-H bond. Particularly, the broad band appearing at ~3250 cm^{-1} is one of the vibrational modes of water and illustrates the level of water desorption at the graphene surfaces. At increasing temperatures, more water molecules desorb from the surface resulting in higher peak intensities. In addition, the IR spectra on H-graphene when cooling down from room temperature to 180 K exhibit a similar change in peak intensity (Figure AIII. 3c), indicating the reversibility of water adsorption. This study reveals that there is more water desorption from H-graphene surface between 180 K and 324 K (right panel) than that for the pristine one (left panel). This supports the proposition that hydrogenation treatment increases the water adsorption on graphene surface.

4.2.4 Near-atmosphere pressure-XPS analysis (NAP-XPS)

Near-ambient pressure X-ray photoelectron spectroscopy (NAP-XPS) was used to analyze the affinity of water towards the surface of graphene upon hydrogenation at a water vapor pressure of 1 mbar. The characterization was conducted directly on the CVD graphene as-grown on copper foil. Figure 4.4a-b shows the C1s and O 1s spectra for graphene samples under ultra-high vacuum (UHV) at a chamber pressure of $<10^{-9}$ mbar. The C1s peak can be deconvoluted into sp^2 C (284.2 eV), sp^3 C (284.8 eV), C-O (286.3 eV) and C=O (288.3 eV) components. The origin of sp^3 C in pristine graphene can be ascribed to the adventitious carbon adsorbed on the surface. The O1s spectrum in UHV can be fitted by three main components: Cu_2O (530.3 eV), O=C (531.3 eV) and O-C (532.3 eV) (Figure 4.4b). The presence of Cu_2O originates from the underlying copper substrate for graphene growth as the employed Al Kα radiation leads to a probing depth of 2-5 nm. At near-ambient pressure conditions in the presence of 1.0 mbar of H_2O, another peak arises at 535.3 eV (Figure 4.4c) which is ascribed to water molecules chemisorbed at graphene surfaces. Specifically, the atomic ratio (at.%) of sp^3 C decreases after 30 s while it increases upon 60 to 120 s of hydrogenation, indicating that hydrogenation treatment not only introduces sp^3 C sites but also can remove surface adsorbents like adventitious carbon (defined as a thin layer of hydrocarbon species).

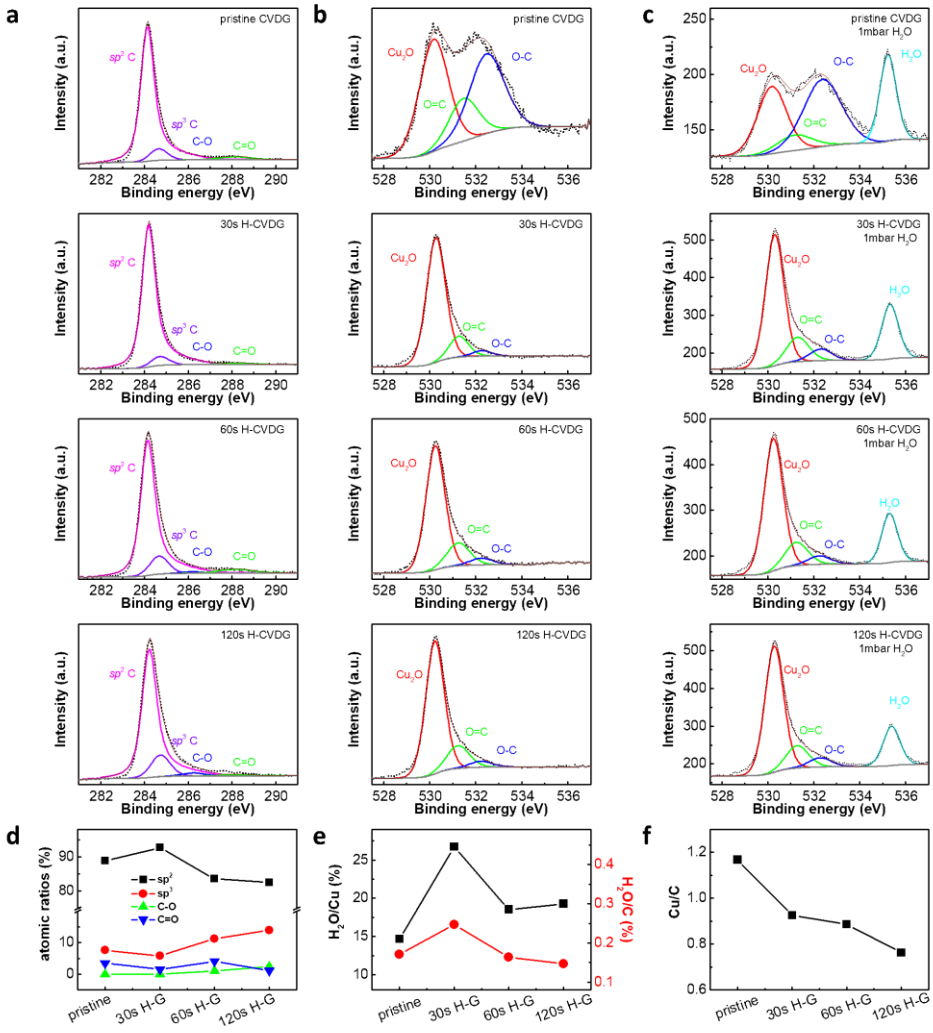

Figure 4.4 Ultra-high vacuum (UHV) and near-ambient pressure (1 mbar H_2O, NAP-) XPS analysis of pristine and hydrogenated CVD graphene (pristine, 30s, 60s, 120s H-CVDG). a) High-resolution carbon (C) 1*s* spectra in UHV. b) High-resolution oxygen (O) 1*s* spectra in UHV. c) High-resolution O 1*s* spectra in the presence of 1 mbar of H_2O. d) Atomic ratios of C 1*s* in UHV. 'Pristine' represents for pristine graphene without hydrogenation after 30, 60, and 120 s of hydrogenation. e) Corresponding atomic ratios of chemisorbed H_2O versus Cu (black) and C (red) obtained from calculating the peak area. f) Ratios of component area of Cu versus peak area of C.

For comparison, the ratios of the component areas of H_2O versus Cu and peak area of C are calculated (Figure 4.4e). The H_2O/Cu ratios are typically higher in H-graphene (H-G, >15 %) when compared to pristine graphene (14.7 %) with 30 s H-G plateaued (26.7 %), suggesting that H-G presents a higher water affinity. On the

other hand, the H_2O/C ratios are higher after 30 s of hydrogenation (from 17.1% to 24.7 %) but lower upon 60 (16.4%) to 120 s (14.7%) of hydrogenation. This observation is consistent with the at.% changes of sp^3 C in Figure 4.4d, confirming the reduction of surface adventitious hydrocarbons especially after 30 s of hydrogenation treatment. As hypothesized, hydrogen radicals can first react with surface adsorbed hydrocarbons before reaching the underlying graphene lattice.[8] To gain more reliable insights, the area ratios of component peaks for Cu and C (calibrated by the corresponding relative sensitivity factor (R.S.F)) are calculated to rule out the influence of adventitious carbon in Figure 4.4f. The gradual decrease of Cu/C ratios points to the fact that hydrogen plasma removes adventitious carbon on graphene which further illustrates the cleaning effects of hydrogenation treatment. In conclusion, hydrogenation of graphene can effectively improve water adsorption, and the highest affinity is found on the surface after a relatively short period (30 s) of hydrogenation treatment.

4.3 Conclusions

Graphene as a two-dimensional surface is prone to be contaminated by airborne hydrocarbons to minimize its surface energy. As confirmed by HRTEM imaging, hydrogenation of graphene can remove partially the adsorbed hydrocarbons without damaging the lattice integrity and crystallinity. Quantitative analysis of TEM images shows that hydrogenated graphene generally presents and keeps a cleaner surface compared to the untreated, pristine samples. Moreover, a water desorption experiment using TPD-IR and XPS characterization in the presence of 1 mbar H_2O further confirmed that graphene adsorbs more water after it has experienced a hydrogenation treatment. In conclusion, hydrogen radicals clean the surface adsorbed hydrocarbons and meanwhile chemically functionalize the underlying graphene lattice from sp^2 to sp^3, resulting in increased water adsorption of H-graphene and thus an anti-fouling effect towards further hydrocarbon contaminations. We therefore believe that cleaning CVD graphene using surface hydrogenation will represent a new standard in device fabrication of graphene sensors, ameliorating the surface chemistry and thus facilitating surface/interface related applications and biosensors.

4.4 References

[1] a) Y.-C. Lin, C.-C. Lu, C.-H. Yeh, C. Jin, K. Suenaga, P.-W. Chiu, *Nano Lett.* **2011**, 12, 414; b) W. Xie, L.-T. Weng, K. M. Ng, C. K. Chan, C.-M. Chan, *Carbon* **2015**, 94, 740.

[2] A. Goossens, V. Calado, A. Barreiro, K. Watanabe, T. Taniguchi, L. Vandersypen, *Appl. Phys. Lett.* **2012**, 100, 073110.

[3] J. Moser, A. Barreiro, A. Bachtold, *Appl. Phys. Lett.* **2007**, 91, 163513.

[4] W. J. Choi, Y. J. Chung, S. Park, C. S. Yang, Y. K. Lee, K. S. An, Y. S. Lee, J. O. Lee, *Adv. Mater.* **2014**, 26, 637.

[5] a) D. Ferrah, O. Renault, C. Petit-Etienne, H. Okuno, C. Berne, V. Bouchiat, G. Cunge, *Surf. Interface Anal.* **2016**, 48, 451; b) Y.-D. Lim, D.-Y. Lee, T.-Z. Shen, C.-H. Ra, J.-Y. Choi, W. J. Yoo, *ACS Nano* **2012**, 6, 4410; c) G. Cunge, D. Ferrah, C. Petit-Etienne, A. Davydova, H. Okuno, D. Kalita, V. Bouchiat, O. Renault, *J. Appl. Phys.* **2015**, 118, 123302.

[6] a) A. Felten, D. McManus, C. Rice, L. Nittler, J.-J. Pireaux, C. Casiraghi, *Appl. Phys. Lett.* **2014**, 105, 183104; b) A. Harpale, M. Panesi, H. B. Chew, *Phys. Rev. B* **2016**, 93, 035416; c) E. Despiau-Pujo, A. Davydova, G. Cunge, D. B. Graves, *Plasma Chem. Plasma Process.* **2016**, 36, 213.

[7] H. Arjmandi-Tash, H. Sokooti, J. Lin, A. Kloosterman, L. Lima, G. F. Schneider, *arXiv preprint arXiv:1707.07941* **2017**.

[8] L. Jiang, W. Fu, Y. Y. Birdja, M. T. Koper, G. F. Schneider, *Nat. Commun.* **2018**, 9, 793.

[9] G. Algara-Siller, O. Lehtinen, A. Turchanin, U. Kaiser, *Appl. Phys. Lett.* **2014**, 104, 153115.

[10] a) A. N. Patel, M. G. Collignon, M. A. O'Connell, W. O. Hung, K. McKelvey, J. V. Macpherson, P. R. Unwin, *J. Am. Chem. Soc.* **2012**, 134, 20117; b) Z. Li, Y. Wang, A. Kozbial, G. Shenoy, F. Zhou, R. McGinley, P. Ireland, B. Morganstein, A. Kunkel, S. P. Surwade, *Nat. Mater.* **2013**, 12, 925.

[11] B. R. Matis, J. S. Burgess, F. A. Bulat, A. L. Friedman, B. H. Houston, J. W. Baldwin, *ACS Nano* **2012**, 6, 17.

[12] Z. Li, A. Kozbial, N. Nioradze, D. Parobek, G. J. Shenoy, M. Salim, S. Amemiya, L. Li, H. Liu, *ACS Nano* **2015**, 10, 349.

[13] P. Y. Huang, C. S. Ruiz-Vargas, A. M. van der Zande, W. S. Whitney, M. P. Levendorf, J. W. Kevek, S. Garg, J. S. Alden, C. J. Hustedt, Y. Zhu, *Nature* **2011**, 469, 389.

[14] C. J. Russo, J. A. Golovchenko, *Proc. Natl. Acad. Sci.* **2012**, 109, 5953.

[15] L. A. Belyaeva, W. Fu, H. Arjmandi-Tash, G. g. F. Schneider, *ACS Cent. Sci.* **2016**, 2, 904.

[16] V. Kofman, M. Witlox, J. Bouwman, I. Ten Kate, H. Linnartz, *Rev. Sci. Instrum.* **2018**, 89, 053111.